Agència de Gestió d'Ajuts Universitaris i de Recerca

UNIÓ EUROPEA
Fons Social Europeu

Memòria justificativa de recerca de les beques predoctorals per a la formació de personal investigador (FI)

La memòria justificativa consta de les dues parts que venen a continuació:
1.- Dades bàsiques i resums
2.- Memòria del treball (informe científic)

Tots els camps són obligatoris

1.- Dades bàsiques i resums

Títol del projecte ha de sintetitzar la temàtica científica del vostre document.
RESEARCH AND DEVELOPMENT OF TERAHERTZ IMAGING SYSTEMS

Dades de l'investigador (benficiari de l'ajut)

Nom
ENRIQUE
Cognoms
NOVA LAVADO
Correu electrònic
ENRIQUE.NOVA@TSC.UPC.EDU

Dades del director del projecte

Nom
JORDI
Cognoms
ROMEU ROBERT
Correu electrònic
ROMEU@TSC.UPC.EDU

Dades de la universitat / centre al que s'està vinculat
UNIVERSITAT POLITÈCNICA DE CATALUNYA / DEPARTAMENT DE TEORIA DE LA SENYAL I COMUNICACIONS / UNITAT ANTENNALAB

Número d'expedient
2010FI_B 00419

Paraules clau: cal que esmenteu cinc conceptes que defineixin el contingut de la vostra memòria.
TERAHERTZ SYSTEMS; FMCW RADAR; RADIOMETRIC SYSTEMS; SECURITY IMAGING; NEAR FIELD IMAGING SYSTEMS

Data de presentació de la justificació
21/01/2011

Generalitat de Catalunya
Departament d'Innovació, Universitats i Empresa

Resum en la llengua del projecte (màxim 300 paraules)

The electromagnetic radiation at a terahertz frequencies (from 0.1 THz to 10 THz) is situated in the frequency band comprised between the optical band and the radio band. The interest of the scientific community in this frequency band has grown up due to its large capabilities to develop innovative imaging systems. The terahertz waves are able to generate extremely short pulses that achieve good spatial resolution, good penetration capabilities and allow to identify microscopic structures using spectral analysis.

The work carried out during the period of the grant has been based on the developement of system working at the aforementioned frequency band. The main system is based on a total power radiometer working at 0.1 THz to perform security imaging. Moreover, the development of this system has been useful to gain knowledge in the behavior of the component systems at this frequency band.

Moreover, a vectorial network analyzer has been used to characterize materials and perform active raster imaging. A materials measurement system has been designed and used to measure material properties as permittivity, losses and water concentration.

Finally, the design of a terahertz time-domain spectrometer (THz-TDS) system has been started. This system will allow to perform tomographic measurement with very high penetration resolutions while allowing the spectral characterization of the sample material. The application range of this kind of system is very wide: from the identification of cancerous tissues of a skin to the characterization of the thickness of a painted surface of a car.

Resum en anglès(màxim 300 paraules)

The electromagnetic radiation at a terahertz frequencies (from 0.1 THz to 10 THz) is situated in the frequency band comprised between the optical band and the radio band. The interest of the scientific community in this frequency band has grown up due to its large capabilities to develop innovative imaging systems. The terahertz waves are able to generate extremely short pulses that achieve good spatial resolution, good penetration capabilities and allow to identify microscopic structures using spectral analysis.

The work carried out during the period of the grant has been based on the developement of system working at the aforementioned frequency band. The main system is based on a total power radiometer working at 0.1 THz to perform security imaging. Moreover, the development of this system has been useful to gain knowledge in the behavior of the component systems at this frequency band.

Moreover, a vectorial network analyzer has been used to characterize materials and perform active raster imaging. A materials measurement system has been designed and used to measure material properties as permittivity, losses and water concentration.

Finally, the design of a terahertz time-domain spectrometer (THz-TDS) system has been started. This system will allow to perform tomographic measurement with very high penetration resolutions while allowing the spectral characterization of the sample material. The application range of this kind of system is very wide: from the identification of cancerous tissues of a skin to the characterization of the thickness of a painted surface of a car.

2.- Memòria del treball (informe científic sense limitació de paraules). Pot incloure altres fitxers de qualsevol mena, no més grans de 10 MB cadascun d'ells.

El trabajo de investigación realizado durante el periodo de disfrute de la beca FI se ha basado en adquirir y desarrollar componentes para la creación de un laboratorio de ondas milimétricas y terahercios en el departamento TSC de la UPC. Una vez se ha dispuesto del laboratorio, se ha empezado a realizar medidas y pruebas para coger experiencia y obtener los primeros resultados con los equipos. Principalmente se han empezado a desarrollar los cuatro sistemas descritos a continuación:

Sistema de caracterización de materiales

Este sistema se basa en utilizar el analizador de redes para caracterizar materiales en la banda de frecuencia de 75 GHz a 110 GHz. El objetivo de este sistema es la medida de características del material como la permitividad o la atenuación. Los equipos utilizados son el analizador, una etapa posicionadora 2D y dos lentes plano-convexas. El haz de microondas se enfoca en un punto donde se coloca la muestra a medir. Si la muestra se coloca en la etapa posicionadora 2D se pueden adquirir imágenes de la muestra que indiquen cambios de sus características dependiendo de la posición.

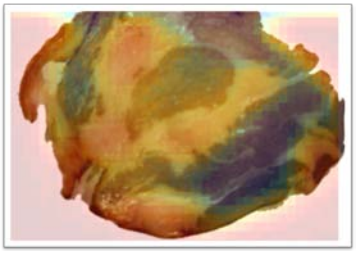

Fig. 1. Caracterización de la concentración de agua de un trozo de embutido

Sistema activo de adquisición de imágenes

A 94 GHz se presenta un compromiso entre capacidad de penetración de materiales y alta resolución espacial que hace de esta banda apropiada para sistemas de imagen de seguridad en tiempo real. La ropa de un individuo es totalmente transparente a estas frecuencias, dejando al descubierto cualquier tipo de arma que lleve debajo de ésta. En el laboratorio hemos desarrollado un sistema activo de adquisición de imágenes. Utilizando el analizador de redes (75 GHz – 110 GHz) y dos posicionadores lineales se pueden obtener imágenes de objetos a través de ropa como la mostrada en la Fig.2.

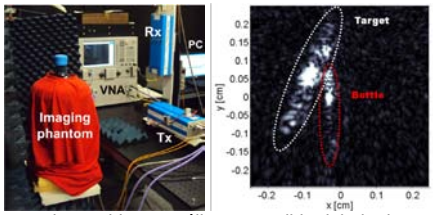

Fig. 2. Imagen de un objeto metálico escondido debajo de una camiseta

Cámara a 94GHz en tiempo real (Radiómetro de potencia total)

Se conoce que las geometrías pasivas tienen la ventaja de que trabajan con una fuente incoherente de señal (la propia radiación emitida por los objetos), siendo inmunes al ruido speckle y a problemas de exposición. Para tener la posibilidad de adquirir imágenes pasivas en banda W (75-110 GHz) se ha desarrollado un radiómetro de potencia total como paso previo al diseño del radiómetro interferométrico. Con este equipo y un sistema de posicionamiento en azimut y elevación se podrán realizar barridos mecánicos para formar imágenes.

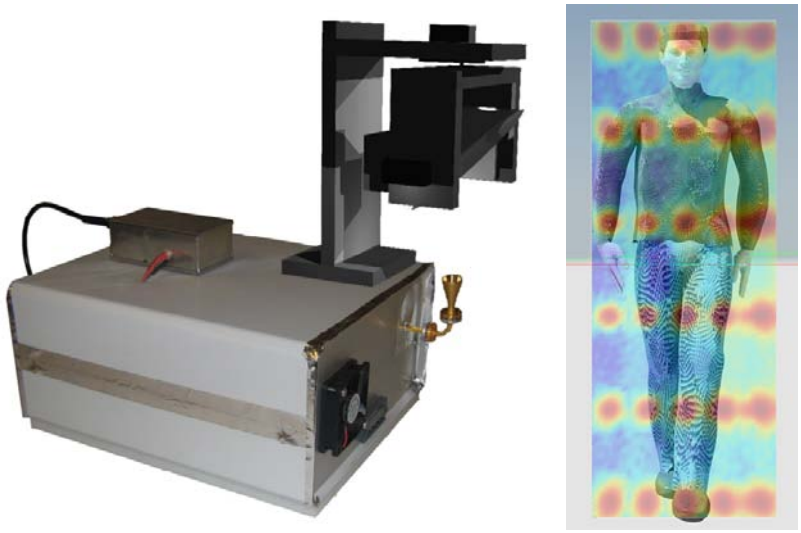

(a) (b)

Fig. 3. (a) Radiometro de potencia total con reflector. (b) Simulación de las capacidades de escaneo del radiometro

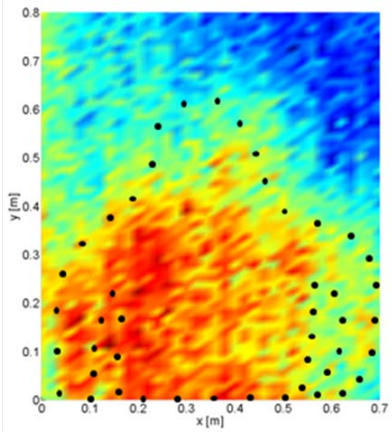

Fig. 4. Imagen preliminar de temperaturas de una persona sentada en una silla obtenida con el radiometro

Sistema de imagen tomográfico a Terahercios

En este periodo se ha iniciado el desarrollo de un sistema de imagen tomográfico. Siguiendo los resultados obtenidos en simulaciones de sistemas de espectroscopia de terahercios, se ha decidido la utilización de sistemas de espectroscopia en el dominio del tiempo para investigar técnicas de adquisición para la obtención de imágenes tomográficas. El rango de aplicaciones de este tipo de sistema es muy amplio: desde la identificación de zonas de tejido canceroso en la piel de un enfermo a la caracterización de una superficie pintada en un coche por ejemplo.

Fig. 5. Sistema de imagen tomográfico en el dominio del tiempo a frecuencia de terahercios

Documentación adjuntada

Publicaciones:

- "Terahertz tomographic imaging technologies", E.Nova, J. Abril, M. Guardiola, S. Capdevila, A. Broquetas, J.Romeu, L. Jofre, URSI 2009
- "THz systems for short-range imaging applications", J. Abril, E. Nova, F. Torres, A. Broquetas, J. Romeu, L. Jofre, URSI 2009
- "Terahertz Subsurface Imaging System", E. Nova, J. Abril, M. Guardiola, S. Capdevila, A. Broquetas, J. Romeu, L. Jofre, EUCAP 2010
- "Terahertz Spectroscopic Material Characterization and Imaging", E. Nova, J. Abril, A. Broquetas, J. Romeu, L. Jofre, URSI 2010
- "Combined Passive and Active Millimeter-Wave Imaging System for Concealed Objects Detection", J.Abril, E.Nova, A.Broquetas, F.Torres, J.Romeu L.Jofre, IRMMW-THz 2010

TERAHERTZ TOMOGRAPHIC IMAGING TECHNOLOGIES

E.Nova , J. Abril, M. Guardiola, S. Capdevila, A. Broquetas, J. Romeu, L. Jofre
romeu@tsc.upc.edu
AntennaLab, Dpt Signal Theory and Communications
Universitat Politecnica de Catalunya

Abstract- **In the context of the TERASENSE Project an imaging system in the terahertz band will be designed and built. The purpose of this demonstrator is to have an in-house developed instrument to test new technologies and carry out proof-of-concept trials of terahertz imaging systems. In this communication a review of the state of the art of terahertz imaging systems and a system specification and layout of the intended system to be constructed at the UPC is presented.**

I. INTRODUCTION

Terahertz imaging systems are potencial canditates for security, biological and sensing applications. The inherent available large bandwidth, and the specific spectral absorption behaviour of certain molecules are key elements in defining the potentialities of such systems [1].

II. STATE OF THE ART

In this section a review of the present state of the art in terahertz imaging systems is presented. According on how the terahertz radiation is generated two different approaches can be readily identified: time and frequency domain systems. In addition the two approaches result in different system performances in terms of frequency resolution and sensitivity. Depending then on the constrains set by the final application one approach is preferred in front of the other.

A. Time domain systems

In terahertz time domain spectroscopy (THz-TDS), short pulses (typically 1-2ps of duration) are transmitted through a sample and measured by gated detection. The Fourier transforms of these pulse shapes are computed in order to obtain the absorption and dispersion coefficients of the sample [2].

Terahertz waves are created using an electrooptic (EO) crystal and/or photoconductive (PC) antennas with mode-locked lasers. The optical pulse width is usually around 100 fs (Fig.1 pulse 1). When the laser beam illuminates the PC antenna, a rapid change in the charge carrier density occurs, and the acceleration of charges results in the formation of THz electromagnetic radiation. This radiation leaves the antenna in the form of a spectrally broadband pulse (Fig.1 pulse 2). The width of the pulse and therefore the bandwidth of the system depends on the laser pulse width and on the lifetime of the charge carriers on the semiconductor. Using an ac-biased low-temperature-grown GaAs (LT-GaAs) PC antenna illuminated by a Ti-sapphire laser, a frequency region of 0.1-15 THz can be covered [3]. An illustration showing the disposition of the emitter, the mechanical delay and the detector is depicted below.

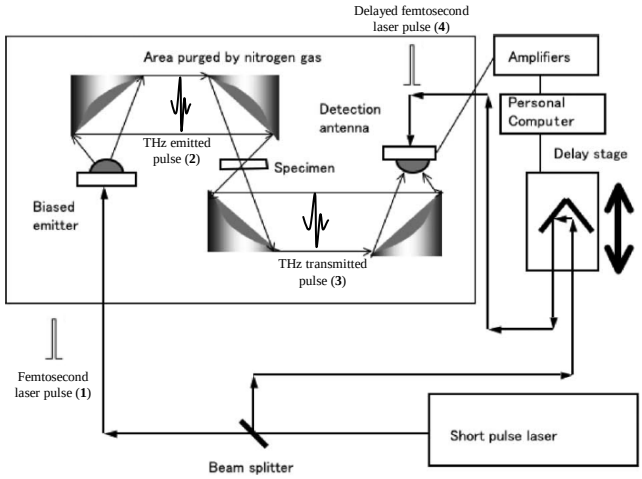

Figure 1. Diagram of a basic THz-TDS system [3].

The emitted THz radiation is collimated and focused onto the sample using parabolic mirrors. The transmitted pulse (Fig.1 pulse 3) is again collimated and focused onto the PC detector. The temporal change of the incident THz pulse can be traced by changing the arrival time of the optical gate pulse (Fig.1 pulse 4). The photocurrent $J(t)$ generated by the incident radiation at time delay *t* is described by the following equation:

$$J(t) = e\mu \int_{-\infty}^{\infty} E(t')N(t'-t)dt' \qquad (1)$$

where $E(t')$, $N(t')$, e and μ are the incident field of THz radiation, the number of photocreated carriers, the elementary electric charge, and the electron mobility respectively. When considering the PC antenna as a sampling detector, the temporal width of $N(t')$ should be as short as possible. $J(t)$ would exactly reflect $E(t)$ if $N(t)$ were a δ-function. The time duration of $N(t)$ is restricted by several factors, such as gating pulse width, momentum relaxation of photocarriers, and carrier lifetime of PC material. With the motivation to shorten the latter, the LT-GaAs has been developed.

The photocurrent obtained from the detector is amplified and processed in a computer. Finally, the Fourier transform

of the pulse is computed in order to obtain the spectrum of the transmitted signal. This spectrum can be compared with the emitted signal spectrum to remove the system response of the experiment. Thanks to the pump-probe coherent detection, SNR levels greater than 10^6 in power are achieved using the described system.

The frequency resolution of the system depends on the measured temporal window. Since the temporal scan is carried out mechanically, there is a trade-off between measurement time and frequency resolution. The resolution achieved with this scheme is around 1 GHz. However, in [4] a system based on an asynchronous optical sampling method is explained, obtaining a frequency resolution of 82.8 MHz with an acquisition time of 10 sec.

Using a scheme similar to THz-TDS, a real-time 2D cross-sectional tomography system is presented in [5]. The method combines the utilization of a two-dimensional free-space electro-optic (ZnTe2) crystal detector and line focusing of the terahertz beam. A 2D spatiotemporal image is captured by a 2D-CCD camera (640x480 pixels) at 10 frames/sec. The transverse resolution is estimated to be 2.5mm at 1 THz whereas the temporal unit increment in the time axis is 14.1 fs/pixel.

This method shows the possibility of developing real-time image acquisition systems in order to monitor moving objects, like products on a belt conveyor or the human body.

B. Frequency domain systems

In terahertz frequency domain spectroscopy (THz-FDS), a continuous-wave THz radiation is produced, transmitted through the material under test, and subsequently measured and analyzed.

The emission is produced through a photomixing of the combined output of two single-frequency diode lasers in a PCS (photo-conductive switch). The wavelength of one (or both) of the lasers is tuned to vary the THz output frequency.
In most spectroscopic applications of photomixing to date, the THz output beam from the PCS has been coupled to a sensitive broadband thermal detector making the overall signal processing incoherent and phase insensitive.

Coherent detection can be achieved at room temperature by mixing the same optical radiation from the diode lasers in a detector PCS onto which the THz signal is also incident. This provides greater sensitivity and faster data acquisition compared to the incoherent technique, and preserves phase information.

A THz-FDS system developed to operate from 210-270 GHz is depicted in [6]. The initial signal is generated by means of a voltage controlled YIG, and then a multiplier chain ending with a broadband sextupler provides several milliwatts of power. The transmitted signal is mixed with a Local Oscillator in a VDI subharmonic mixer (wr3.4SHM). The resulting Intermediate Frequency (IF) at 1.7 GHz is then amplified, detected, and read by a computer. The heterodyne receiver which measures the transmission through materials under test yields an accuracy better than 0.5%.

A highly-integrated dual semiconductor laser Module (Fig. 2), using two ErAs:GaAs photomixers, and based on THz-FDS is described in [7]. The system utilizes a single package integration of two 783 nm distributed feedback laser diodes (DBF) with a high-resolution wavelength discriminator. Digital signal processing electronics provide precise frequency control and yield ~200 MHz accuracy of the THz signal frequency. Continuous mode hop-free frequency sweeping is demonstrated with < 1 GHz resolution from 200 GHz to 1.85 THz. The highly efficient CW nature of the photo-mixing source puts all the THz power at the frequency of interest, yielding excellent signal-to-noise ratio of 80 dB/Hz at 200 GHz and 60 dB/Hz at 1THz .

To measure the laser frequencies, 20% of the primary beam is coupled through an optical filter that has a predetermined wavelength profile and is then incident on a photodiode.

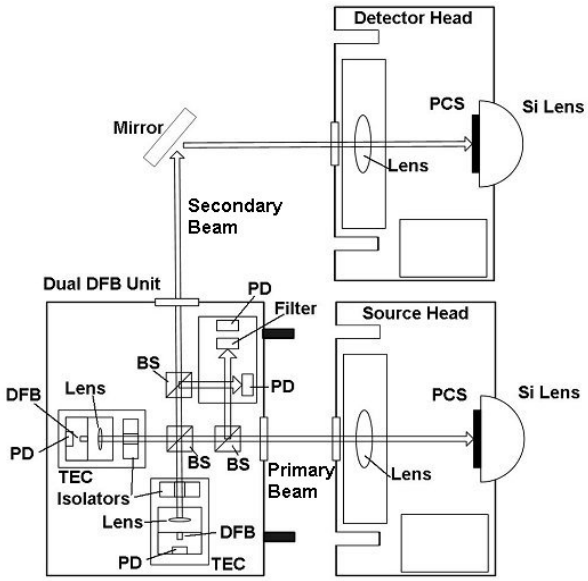

Figure 2. Integrated source and detector module drawing [7].

Comparing both techniques, some of the benefits of the coherent frequency-domain technique compared to the time-domain technique are: (1) no moving parts (i.e. no mechanical scanning delay line), (2) higher frequency resolution, and (3) the ability to selectively scan specific frequency regions of interest with adjustable resolution. Mention that, unlike pulsed systems, CW photomixing results in all of the THz power being concentrated at a single THz frequency, thus improving spectral density and signal- to-noise ratio at that frequency. However, previously it has been difficult to realize practical frequency-domain spectrometers due to the challenges associated with the construction and control of the dual lasers, namely mode-matching and collimation of the two laser beams and precise control of their difference frequency.

In the table below, the most important parameters of the THz systems are shown. The wider frequency range of the THz-TDS compared with THz-FDS can be pointed out. However the resolution of the latter is higher.

TABLE I
Comparison between relevant parameters of time domain and frequency domain systems

Parameter	Time domain	Freq. domain
Freq. range	100 – 15000 GHz	100 – 2000 GHz
Output power	~ 2uW	~ 1 uW
Sensitivity	-	10^{-12} – 10^{-10} W/Hz

Freq. resolution	~ 1 GHz	~ 0.1 GHz
SNR	~ 10^6	$10^6 – 10^8$
Spectral purity	-	0.010 – 0.25 GHz

III. A PROPOSAL FOR THE UPC SYSTEM

The imaging system proposed at the UPC is conceived to present high flexibility when measuring a field distribution in a planar surface. To do it, the system is based on the MST (Modulated Scattering Technique) approach, which reduces the RF equipment necessary for each pixel of the planar surface, and only requires of low frequency wiring. The main part of the system consists of a planar probe array, named retina, which is placed in between the object under test and the detector. A source transmits an incident field in the range of THz frequencies towards a parabolic mirror, which de-collimates the beam towards the sample to be imaged. A second parabolic mirror collimates the scattered fields into the detector.

The sample has been placed on a rotary stage, to be able to select the desired direction to perform the imaging. The field which is being imaged is measured by the retina placed between the sample and the receiving parabolic mirror. When the retina is illuminated by the transmitted field, each of its probes (pixels) back-scatters a signal marked in a pre-defined way, and therefore becomes distinguishable from the rest. In this way, from the received signal it is possible to obtain information about the scattered fields at each of the pixels. The marking is done by placing at each of the probes a NEMS switch capable to change the load status of the probe according to an external signal.

As a first design step, a 25-50 GHz imaging system is being developed using the same principle as described in the following paragraph. In this case, the retina is planar antenna array composed by 16 pixels which are activated independently using NEMS switches at their center. The illuminator and the collector are horn antennas providing a known electromagnetic field distribution.

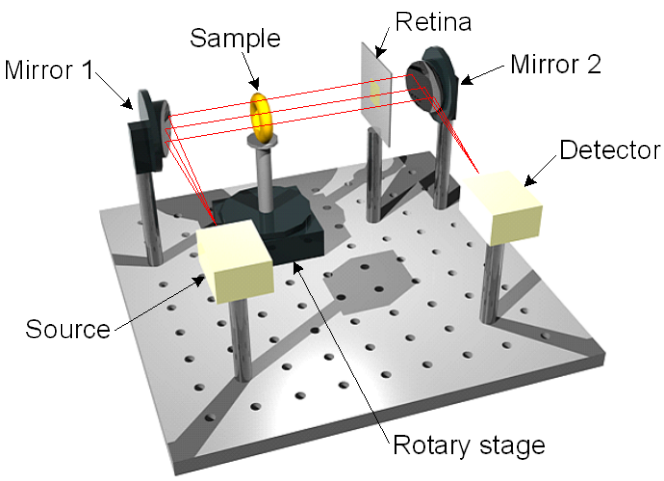

Figure 3: THz imaging system proposal.

IV. CONCLUSIONS

THz imaging systems are inherent UWB systems. The potentiality to obtain high resolution images has already been realized. A major challenge is the fast sampling of EM field distribution to produce real time images. A MST based retina will be tested in THz imaging system.

ACKNOWLEDMENTS

This work was supported in part by Spanish CICYT under projects TEC2004-04866-C04-02 and TEC2007-66698-C04-01 and CONSOLIDER CSD2008-68.

REFERENCES

[1] L.Jofre, A. Broquetas, J. Romeu, S. Blanch, A. Papio, X. Fabregas, A. Cardama, *"UWB Tomographic Radar Imaging of Penetrable and Impenetrable Objects"*, Proceedings of the IEEE, vol. 97, no. 2, February 2009

[2] Mira Naftaly, Robert E. Miles, *"Terahertz Time-Domain Spectroscopy for Material Characterization"* , Proceedings of the IEEE, vol. 95, No. 8, August 2007

[3] Iwao Hosako, Norihiko Sekine, Mikhail Patrashin, Shingo Saito, Kaori Fukunaga, Yasuko Kasai, Philippe Baron, Takamasa Seta, Jana Mendrok, Satoshi Ochiai, Hiroaki Yasuda, *"At the Dawn of a New Era in Terahertz Technology"*, Proceedings of the IEEE, vol. 95, No. 8, August 2007

[4] Eisuke Saneyoshi, Takeshi Yasui, Tsutomu Araki, *"Rapid, Ultrahigh-resolution Terahertz Time-domain Spectrometer Using Two Asynchronous-controlled Femtosecond Laser"s*, IRMMW-THz, vol. 1, pag. 317-128, September 2005

[5] Takeshi Yasui, Takashi Yasuda, Tsutomu Araki, *"Real-time Two-dimensional Terahertz Tomography"*, IRMMW-THz, vol. 2, pag. 580-581, September 2005

[6] David S. Kurtz, Thomas W. Crowe, Jeffrey L. Hesler, David W. Porterfield, *"Frequency Domain Terahertz Spectroscopy"*, Virginia Diodes Inc., IEEE 2005.

[7] Joseph R. Demers, Ronald T. Logan Jr., Elliot R. Brown, *"An Optically Integrated Coherent frequency-Domain THz Spectrometer with Signal-to-Noise Ratio up to 80 dB"*, 1-4244-1168-9 IEEE, 2007

THZ SYSTEMS FOR SHORT-RANGE IMAGING APPLICATIONS

J. Abril, E.Nova, F.Torres, A. Broquetas, J. Romeu, L. Jofre
broquetas@tsc.upc.edu
Remote Sensing Lab, Dpt. Signal Theory and Communications
Universitat Politecnica de Catalunya

Abstract- **The lower frequency range of THz band is appropriate for short range imaging applications offering a good compromise between spatial resolution, media attenuation and technology availability. In the framework of the TERASENSE project alternative approaches based on passive and active systems are proposed and studied in order to develop suitable demonstration prototypes.**

I. INTRODUCTION

The millimeter wave (MMW) band of frequencies extends from 30 GHz to 300 GHz, whereas terahertz (THz) band extends from about 0.1 to about 3 THz. In short range imaging applications like security checkpoints in airports or non destructive testing of materials the transition frequency range between MMW and THz offers a good compromise between spatial resolution and tolerable media attenuation. Due to the short wavelengths involved a good spatial resolution in the order of few centimetres or better can be achieved even with small apertures. Moreover around 100 GHz essential imaging subsystems like oscillators, low noise amplifiers, mixers, etc. are commercially available. In this context the paper contains a review of the state of the art involving both imaging methodologies active and passive and underlying technologies. Both passive and active imaging prototype systems are being studied, the paper presents the basic operation principles and geometries of exploration considered and the main technical requirements related to performance parameters such as spatial resolution, sensitivity, etc.

II. STATE OF THE ART

In this section a review of the current state of the art in short-range terahertz imaging systems is presented. In the following two sections both active and passive techniques are depicted including the required technologies.

A. Active systems

Active MMW imaging methods are based on a transmitter-receiver model usual in imaging radar. The image of the illuminated scene is formed from the measured scattered signals.

In spite of the technological complexities associated with the lower range of THz, a variety of solid-state and beam wave tubes sources exist. Examples of vacuum-tubes MMW sources are the travelling-wave tube (TWT) and the backward-wave oscillator (BWO). Among the solid-state sources available, we can find the Gunn diode and the Impact-Ionization Transit-Time (IMPATT) diode oscillators.

Tube sources are mainly used for high power applications up to 22kW in CW. The BWO can operate at frequencies up to 1.3 THz and the are widely used in spectroscopic applications.

Gunn oscillators are available at frequencies up to 140 GHz in the InP version. Due to the low power output of few milliwatts and to the low-noise behaviour, these devices are useful as local oscillators. IMPATT oscillators have higher output power but also higher noise outputs compared with Gunn devices.

However, HEMT transistors are supplanting Gunn and IMPATT in many applications, especially at the lower frequencies. In the HEMT oscillators, the gain can be controlled and the DC to RF efficiency is higher than using diode devices. An oscillator working at a frequency up to 346 GHz has been developed using a 35nm InP HEMT transistor [1], however only 25uW of output power can be reached in this case.

The receiver RF front-end usually consists on a Schottky-barrier diode used to detect the incoming signal. Thanks to the higher contrast achieved with the artificial illumination, the receiver does not have to be extremely sensitive. The basic approach is to use a single detector with a mechanical scanning. However, for practical purposes, array detectors are preferable in order to shorten the scanning time. A beamwidth of 2.3 degrees with 20 dB peak to null ratios can be achieved with an array of 64 elements at 94 GHz [2].

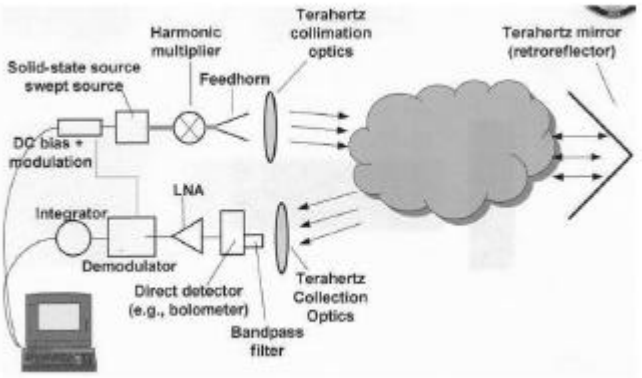

Figure 1. Diagram of an active MMW radar for detecting atmospheric species [5].

Figure 1 presents the diagram of a typical THz radar. The source is a low frequency source multiplied by an harmonic multiplier (i.e. a varactor). The detector consists in a bolometer plus an amplification and demodulation stage. The bolometer is a commonly used device for signal detection in the far-infrared and THz bands.

In order to guide the radiation it has to be pointed out that at frequencies above 100 GHz, metal waveguides become unacceptably lossy due to skin effect losses and the inability to fabricate the waveguides with enough precision required for low loss operation. This limitation can be overcome by using techniques developed for the visible and the infrared portions of the spectrum. This approach has been called "quasi-optics". It is possible to build optical analogs of almost all waveguide components like waveguides, attenuators, polarization rotators, directional couplers and antennas. Almost zero loss can be achieved if the waveguide is made from mirrors. Nevertheless, MMW optical components in general are bulky.

A variety of MMW active imaging techniques have been already published. [3] presents an imaging method based on multi-parametric encoded illumination. The image contrast is enhanced by using an active system fed by three BWOs in order to sweep the frequency of the source from 52 GHz to 178 GHz. Moreover the coherent noises and distortions are reduced by accumulating distinct coherent images. These images are captured by a receiving array of microstrip log-periodical antennas disposed in the image plane of the focusing element.

A 2-D acoustic phase imaging system is presented in [4]. Metallic and dielectric materials can be detected by measuring their acoustic phase with electromagnetic radiation. The acoustic phase of a vibrating object is measured using homodyne mixing, therefore the interference between the reflection from the object and a reference signal is detected.

A resolution of 2mm is achieved with this technique, which is better than the diffraction limited resolution of 3 mm. Since it is a differential detection method, the background is not distinguished. Furthermore, objects with similar contrast as the background can be identified.

B. Passive systems

Passive Millimeter wave imaging (PMMW) systems are usually characterized by their thermal and the spatial resolutions. The development of such systems is driven by security applications like the detection of vehicles behind camouflage materials or concealed weapon detection at airports or other public buildings. Thus, using passive MMW has a major advantage in these environments since it does not suffer from scattering and multipath propagation, as compared to active (radar) imaging.

A critical issue to be considered in MMW imaging systems is the acquisition time to get a full image, hence, different systems can be found in the literature, due to the distinct application requirements.

Up to date, no un-cooled solid-state millimeter-wave detector has achieved sufficient sensitivity to directly measure terrestrial scene brightness temperatures with video-rate thermal resolution useful for the described applications. By way of example, semiconductor detectors such as hetero-structure diodes have reached sensitivity levels such that a single monolithic millimeter-wave integrated circuit (MMIC) amplifier chip preamplifier can provide the power required for video-rate focal plane imaging. For instance a focal-plane array with 25k (128 x 192) pixels requires the use of 25,000 such MMIC amplifiers. The same scenario but using the corresponding phased-array camera at a 30 Hz frame rate, needs less than 1,300 MMIC amplifier chips [6][7].

However, as a consequence of recent developments in the market, communication technologies and computers are capable of processing a larger amount of data at very high speed. This enables digital beam-forming (BF) imager architecture to be realized; so that BF-PMMW imager based on high-speed digital signal processor (DSP) and a conformal array of planar antennas may shrink the large volume foot print of existing quasi-optical PMMW imagers to a thin panel a few millimetres thick, increasing the applicable scenarios. Moreover, using low cost packaging and assembly methods employed in mobile computer technology, the final cost of the imagers could decrease drastically [8]. Unlike the conventional imaging which uses quasi-optical beam former, a focal plane array and receivers, in that order, Fig. 2, and that yields a system volume ~D^3; electronic imaging, the beam-former is situated after the receivers (DSP) yielding instead a system volume ~2?D^2. Besides, the very serious depth of field limitation of a few centimetres for short range (< few metres) quasi-optical security portals can be overcome by creating multiple near-field images electronically on a frame rate time-scale.

With regard to the array techniques, minimally redundant arrays are of interest in electronic beam-forming as they sample all scene spatial frequencies across an aperture with the minimum number of receiver elements [9]. Taking this into account, a comparison of radiometric sensitivities for a mechanical and electronic imager has shown better results for the latter [8].

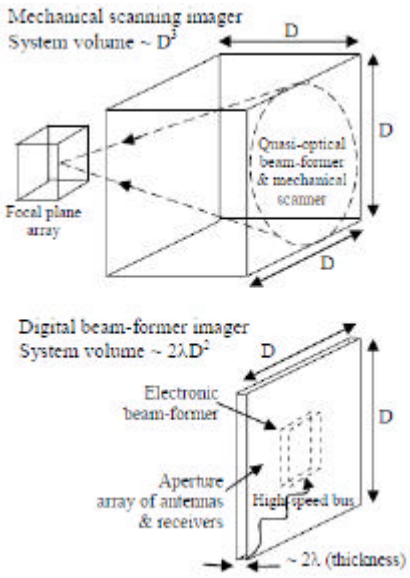

Figure 2. Mechanical scanning imager (upper), electronic scanning imager (lower) [8].

Among other important projects in PMMW field, a programme supported by the UK Department of Trade and Industry (DTI) to develop pre-competitive technology is working on electronic imaging for commercial security applications. Described in [8], a demonstrator is been developing, having a real-time imaging (25 fps) capability, with a sensitivity (≤ 1 K), comparable to existing PMMW imaging systems. Maximum utility for minimum cost is sought by operating at a low radio frequency (22.5 GHz) and having a moderate radio frequency bandwidth (300 MHz) in a heterodyne architecture and by using a small number of receiver channels (32).

Generally two types of antenna are chosen for investigations, namely short horn antennas due to the relatively simple design procedures and reproducible high quality beam patterns and patch antennas due to the low cost production and ease of integration with multilayer electronic circuits.

Some other variations of PMMW using additional ideas can be found in the literature, such as a system with rotating space observation method [10], or another one with white noise illumination for concealed weapons detection [11], which offers interesting advantages and solutions. This technique is useful mainly in indoor environments where the brightness temperature contrast does not exceed 5-15K, employing artificial MMW radiation sources in order to increase the contrast. Table I contains a summary of the main typical technical characteristics of both passive and active short range imaging systems.

TABLE I
Comparison between relevant typical parameters of Active MMW and Passive MMW systems

Parameter	AMMW	PMMW
Freq. range	35,94,140,220 GHz	22.5-94 GHz
Output power	~ 2mW	-
Sensitivity	-	=1 K
Bandwidth	CW	Up to 10 GHz
Spatial resolution	~ 2.5 mm	5.2 milliradians
Target distance	1-5 m	0.05-5 m
Time imaging	Up to 25 fps	Up to 25 fps

III. UPC PROTOTYPES UNDER STUDY

The absence of illumination in passive systems is a key aspect to achieve a public acceptance of imaging devices for security screening applications in airports and other sensitive facilities. However active systems can exhibit better sensitivity, imaging speed and spatial resolution. For these reasons both passive and active approaches are being evaluated both by means of simulations and experimentally.

III.A Passive Prototype

The proposed passive prototype is based on the aperture synthesis technique. This concept was developed for radioastronomy applications [12] and has recently been assessed in the framework of the ESA SMOS mission [13]. This approach minimizes the number of receivers needed to form an image since N receivers can produce an image of N(N-1) pixels (some of them redundant). Note that in the case of focal plane radiometers a receiver is needed for each image resolution cell if mechanical or electronic scanning is avoided.

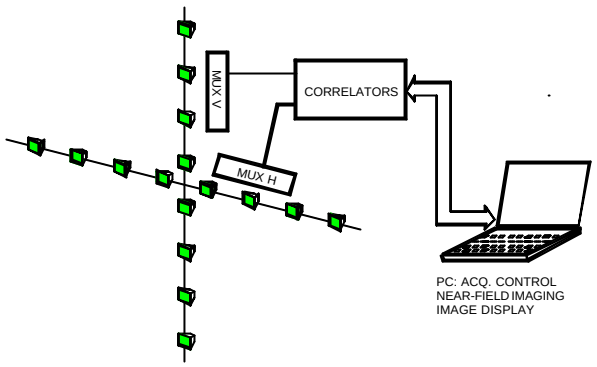

Figure 3. Aperture Synthesis imaging radiometer intended for security screening of population and luggage in airports and other sensitive facilities.

Fig. 3 shows a possible geometry of acquisition based on two crossed linear arrays, other geometries are possible such as the "Y" shape with three arms at 120 degrees angular spacing. The noise signals delivered by every antenna element must be amplified and down-converted to base band I/Q channels and digitised. The received signals can be delivered to a FPGA correlator board using a fast serial bus to minimize interconnection costs. In an ideal case, the correlations of all the antenna pairs are directly related to the Fourier Tranform of the scene brightness temperature. In fact this is true for scenes in the far field of the array. For security applications the scene is at short distance of the array, but still it is possible to invert the correlation data in order to properly focus the image in near-field [14][15]. The main parameters of a first prototype are being studied to assess the viability of real-time operation.

III.B Active Prototype

Several configurations are feasible for active imaging of security scenes. The linear crossed arrays considered for passive imaging can in fact easily operate in an active configuration.

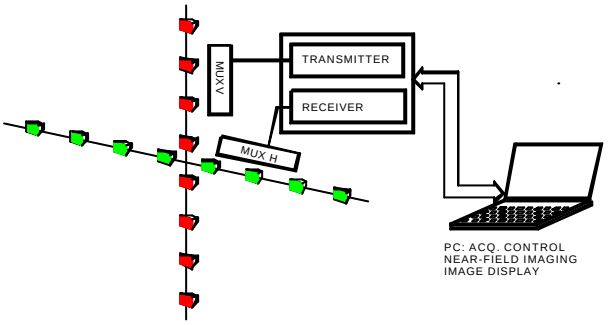

Figure 4. Active imaging based on the linear crossed arrays.

This is shown in Fig. 4 where the antennas belonging to the vertical array are used sequentially for the scene illumination whereas the elements of the horizontal array are used to receive the scattered signals from the scene to be imaged.
A focusing operator can be used based on the inversion of the theoretical scattered field amplitude and phase between each point of the scene and the transmitting and receiving positions [16].

An alternative approach which simplifies the front-end is based on using a reconfigurable reflectarray which can be designed using MEMS or LCD technologies [17]. In this case (Fig. 5) the focusing required to form the image is provided by dynamically programming the appropriate weights in the reflectarray elements. Up to date planar arrays have been investigated for satellite communication antennas and near-field imaging purposes. Using conformed surfaces it is possible to minimize the phase changes required to scan the intended scene which simplifies the reflectarray design and programming. Key aspects of the LCD are the introduced losses, phase range and switching speed. The pros and cons of the different approaches are being determined and balanced to obtain a first feasible prototype.

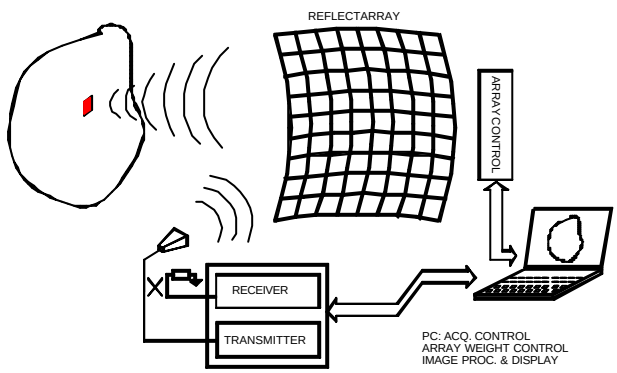

Figure 5. Active imaging based on a conformed reflectarray.

IV. CONCLUSIONS

Several passive and active configurations are able to provide high resolution imaging in short range applications using the lower part of the THz band. From a first simulated analysis a first prototype using linear arrays of antennas or a reflectarray technology will we developed and tested.

ACKNOWLEDMENTS

This work was supported in part by Spanish CICYT under projects TEC2004-04866-C04-02 and TEC2007-66698-C04-01 and CONSOLIDER CSD2008-68.

REFERENCES

[1] V.Radisic, X.B.Mei, W.R. Deal, W. Yoshida , P.H. Liu, J. Uyeda, M. Barsky, L. Samoska, A. Fung, T. Gaier, and R. Lai, *"Demonstration of Sub-Millimeter Wave Fundamental Oscillators Using 35-nm InP HEMT Technology"*, IEEE Microwave and Wireless Components Lett., vol. 17, No. 3, March 2007

[2] Sowers, J.; Byer, N.; Edward, B.; McPherson, D.; Weinreb, S.; Rucky, F., *"Electronically steered, receive monopulse, active phased array at 94 GHz"*, EEE MTT-S International, vol. 3, pag. 1581 - 1584, Jun 1996

[3] Volkov, L.V. Voronko, A.I. Volkova, N.L. Karapetyan, A.R. , *"Active MMW imaging technique for contraband detection"*, Microwave Conference, 2003. 33rd European, vol. 2, pag. 531-534, Jun 1996

[4] Redo-Sanchez, A. Kaur, G. Xi-Cheng Zhang Buersgens, F. Kersting, R., *"2-D Acoustic Phase Imaging With Millimeter-Wave Radiation"*, Microwave Theory and Techniques, IEEE Transactions on, vol. 57, pag. 589-593, March 2009

[5] R. W. McMillan, *"Terahertz Imaging Millimiter-Wave Radar"*, U.S. Army Space and Missile Defense Command, Huntsville, Alabama, USA

[6] Jürgen Ritcher, Denis Nötel, Frank Klöppel, Johan Huck, Helmut Essen, Lorentz-Peter Schmidt, *"A Multi -Channel Radiometer with Focal Plane Array Antenna for W-Band Passive Millimeter-wave Imaging"*, IEEE 0-7803-9542-5, 2006.

[7] John A. Lovberg, Chris Martin, Vladimir Kolinko, *"KVideo-Rate Passive Millimeter-Wave Imaging Using Phased Arrays"*, IEEE 1-4244-0688-9, 2007

[8] N.A. Salmon, J.Beale, J. Parkinson, S.Hayward, P.Hall, R.Macpherson, R. Lewis, A. Harvey, *"Digital Beam-Forming for Passive Millimeter Wave Security Imaging*, IEEE 2008

[9] Meurisse, Y and Delmas, JP, *'Bounds for Sparse Planar and Volume Arrays'*, IEEE Trans. On Information Theory, Vol. 47, No. 1, January 2001

[10] D.O. Korneev, L.Yu. Bogdanov, A.V. Nalivkin, *"Passive Millimeter Wave Imaging System with White Noise Illumination for Conceled Weapons Detection"*, IEEE 0-7803-8490-3, 2004

[11] D. 0. Komeev, L.Yu. Bogdanov, A.V. Nalivkin, *"Passive Millimeter Wave Imaging System with White Noise Illumination for Concealed Weapons Detection"*, Joint 29th - Int. Conf. on Infrared and Millimeter Waves and 12th Int. Conf. on Terahertz Electronics, 2004.

[12] A.Thompson, J.Moran, and G. Swenson, *"Interferometry and Synthesis in Radioastronomy"*. John Wiley and Sons, 1986.

[13] M.Martín-Neira and J. Goutoule, *"MIRAS: a two dimensional aperture synthesis radiometer for soil moisture and ocean salinity observations"*. ESA Bulletin, vol. 92, pp. 95-104, 1997.

[14] A. B. Tanner, F. Torres, B. H. Lambrigsten, T. M. Gaier. "*Near Field characterization of the GeoSTAR demonstrator*". International Geoscience and Remote Sensing Symposium IGARSS 2006. pp. 2529-2532. Denver, Colorado. USA. 2006

[15]. M. Peichel, H. Suess, M. Suess, *"Microwave imaging of the brightness. temperature distribution of extended areas in the near and far field using two-dimensional aperture synthesis with high spatial resolution"*, Radio Science, Vol. 33, N. 3 pp. 781-801 May-June 1998.

[16] J.M. Girones, L. Jofre, M. Ferrando, E. de los Reyes, J.Ch. Bolomey, *"Microwave imaging with crossed linear arrays"*, IEE PROCEEDINGS, Vol. 134, Pt. H, No. 3, JUNE 1987, pp.249-252.

[17] Encinar, J.A.; Arrebola, M.; Toso, G., *"Design of a Tx/Rx Reflectarray Antenna for Space Applications"*, The Second European Conference on Antennas and Propagation, 2007. EuCAP 2007, 11-16 Nov. 2007 Page(s):1 – 5.

Terahertz Subsurface Imaging System

E. Nova, J. Abril, M. Guardiola, S. Capdevila, A. Broquetas, J. Romeu, L. Jofre,
AntennaLab, Signal Theory and Communications Dpt.
Universitat Politècnica de Catalunya
Jordi Girona 1-3, Barcelona, 08043, Spain
{romeu, enrique.nova}@tsc.upc.edu

***Abstract*— A subsurface imaging system based on a terahertz time-domain spectrometer (THz-TDS) is described in this paper. The system performance has been simulated in terms of spatial resolution, penetration capabilities and SNR. Moreover, a commercial THz-TDS has been used to perform the proof-of-concept of the described system.**

I. Introduction

Terahertz imaging systems are gaining relevance in the field of electromagnetic imaging thanks to their good compromise between spatial resolution and penetration capabilities. The inherent available large bandwidth and the specific spectral absorption behavior of certain molecules are key elements in defining the potentialities of such systems. Moreover, the recent evolution of electromagnetic sources working at this frequency band opens a new scope of applications to be developed using terahertz radiation. Since most non-polar, non-metallic materials are relatively transparent to terahertz radiation, non destructive testing can be performed through their surfaces. Furthermore, the available terahertz time domain spectroscopy systems emit narrow pulses with large spectral content approximately from 0.3 THz to 3 THz. Hence, these systems are well suited to perform subsurface imaging since they can yield depth resolutions in the order of few micrometers.

In the next sections, a subsurface imaging setup based on a THz-TDS system is proposed and simulated in order to foresee its performance. Furthermore, in order to validate the simulations a set of measurements have been performed using a commercial THz spectrometer.

II. Setup Geometry

Fig.1 shows the proposed system diagram [1] based on a terahertz time-domain spectroscopy system. In this scheme, the measurements are done in reflection. Terahertz radiation is created at the transmitting photoconductive antenna (Tx PCA), collimated by a mirror and aimed to the sample. The reflected scattered fields produced by the incident beam are guided towards a retina using a beamsplitter.

The retina is able to recover the value of electric field at the position of each element using the modulated scatterer technique (MST) [2].

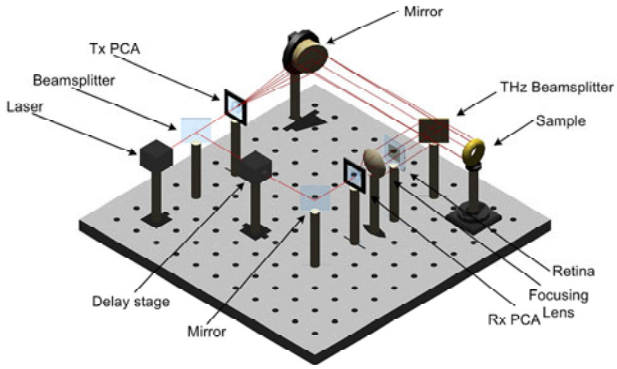

Fig.1: THz subsurface imaging system

In Fig.2, the design of the retina is presented. It is composed by 8x8 UWB elements. A Nano Electromechanical System (NEMS) [3] is placed at the center of each element, changing its load status depending on the NEMS state. Hence, using the variation of the element load status, the field can be modulated at its position and therefore measured using the MST technique.

Once the electric field has crossed the retina, it is focused onto the receiving photoconductive antenna (Rx PCA) using a lens. A probe pulse is taken from the source laser and delayed using a controllable mechanical delay stage. The sampling of the terahertz electric field at the receiving antenna is controlled by the probe pulse, enabling a coherent detection of the incident THz radiation. Finally, the current created at the Rx PCA is amplified using a lock-in amplifier and processed using the FFT to obtain the spectral content of the pulse.

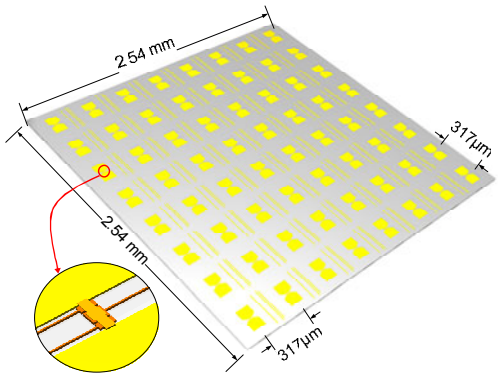

Fig.2: Retina layout and dimensions

III. Simulation Results

In order to predict the performance of the system, simulations of the image reconstruction algorithm have been carried out. Once the field distribution along the retina is known, a focusing algorithm is applied to reconstruct a transversal image. The simulations have been performed using an FDTD electromagnetic simulator [4]. A 16x16 array of probes spaced λ/2 at 1 THz have been used to recover the field at 2 mm from the object. A Gaussian pulse with spectral content from 500 GHz to 1.5 THz has been used as excitation. The equation (1) has been applied to focus the field, where $\tilde{\psi}(x,y)$ is a reconstructed image pixel, $E(x',y';f)$ is the electric field value at the probe placed at coordinates (x',y') and $r_{x,y}(x',y')$ is the distance from the probe to the pixel.

$$\tilde{\psi}(x,y) = \sum_{f}\sum_{x',y'} E(x',y';f)\cdot e^{jk\cdot r_{x,y}(x',y')} \qquad (1)$$

Fig. 3 shows the results of the simulation of a perfect electric conductor (PEC) block of 2x2 mm. The shape of the object is perfectly recovered. Moreover, the existence of a crack on the surface can be also exposed.

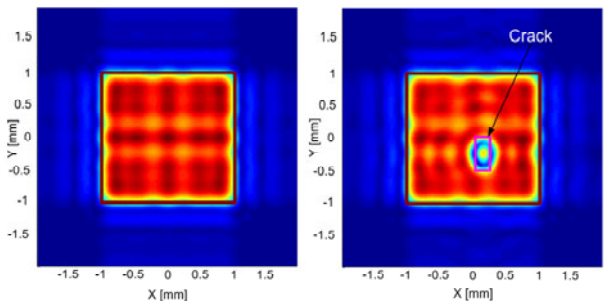

(a) (b)

Fig.3: Reconstructed image from a PEC block of 2x2 mm (a). In (b), a crack of 0.2x0.5x0.3 mm has been added to the block simulated in (a).

Spectral imaging simulations have been also carried out. A strip of lossy dielectric material of 0.4x1 mm has been inserted into a lossless dielectric block of 1x1 mm. The permittivity value for both materials is ε_r=4, however the strip material has an absorption peak at 1 THz with a complex permittivity of ε_r=4+j9 at this frequency. Fig. 4 (a) shows the results of a simulation using the full excitation bandwidth whereas in Fig. 4(b) only a frequency band from 975 GHz to 1025 GHz is used to reconstruct the image. The strip can be revealed when a narrow bandwidth around the strip absorption frequency is used. Furthermore a complete spectral response of each pixel can be obtained.

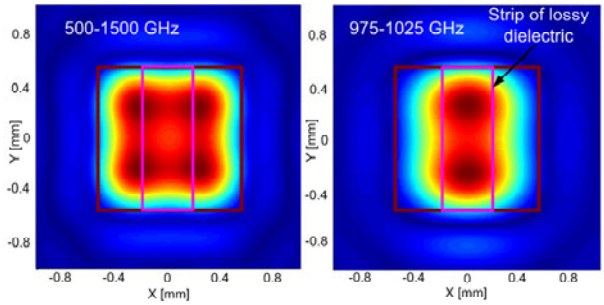

(a) (b)

Fig.4: Image reconstruction of a lossy dielectric embedded in a lossless block. (a) presents a complete reconstruction using the full bandwidth, (b) shows the reconstruction using only information around the peak absorption band.

IV. Setup Characterization

The SNR at the receiver has been characterized for different values of the sample dielectric permittivity. A source power of 20 μW and a 15% of coupling efficiency have been considered [5]. Thus, a beam power of 3 μW can be obtained. The multiplexing losses due to the retina are 18 dB whereas the losses due to the field modulation have been considered 6 dB. The noise current at the receiving photoconductive antenna is $1.3\cdot10^{-13}$ A rms. The losses due to atmospheric absorption and retina absorption have been neglected in front of the multiplexing losses. With these values, the achieved SNR curves for permittivity values of ε_r=40, ε_r=20 and ε_r=5 are depicted against total integration time for the 8x8 element retina in Fig. 5.

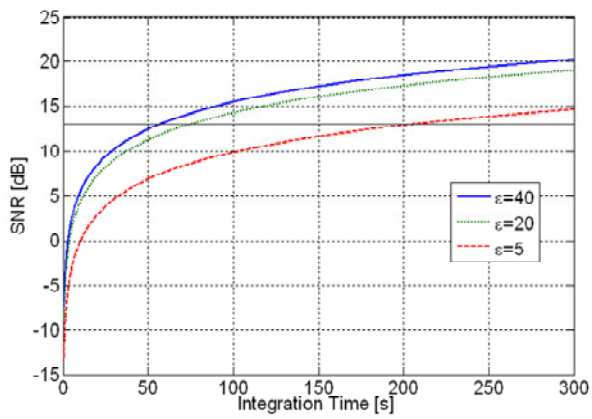

Fig.5: Achieved SNR against integration time for different sample dielectric constants

The minimum required value of SNR necessary to obtain an image has been considered 13 dB. Hence, the integration time needed to reconstruct the full image will be 57 s, 75 s and 206 s for ε_r=40, ε_r=20 and ε_r=5 respectively.

V. Measurements

A. Measurement setup

A portable THz-TDS system [6] has been used to obtain raster images in reflection. This spectrometer allows to measure in real time with a dynamic range of around 25 dB and a repetition rate greater than 7 Hz. Nevertheless, the aforementioned value of dynamic range can be improved if the measurement is averaged for several acquisitions.

The transmitted pulse has approximately 2.5 THz of bandwidth. Therefore a depth resolution of about 60 µm is achieved when measuring in reflection. Fig. 6 shows the setup geometry used to obtain the images presented in this section. The spectrometer is fixed on an optical breadboard whereas the sample is held on a 3D stage composed of three independent linear stages. Using the linear stage in Z direction, the sample can be placed at the focus of the lens where the measured beam waist is 170 µm; therefore at this Z position a pixel resolution of 340 µm is obtained.

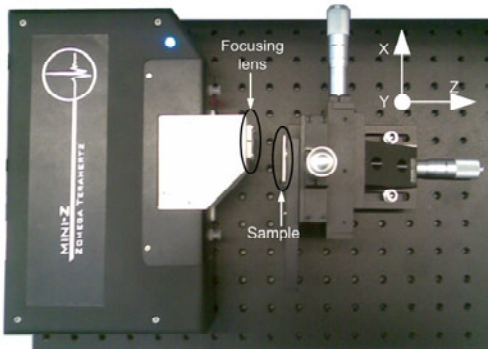

Fig.6: Photograph of the measurement setup

The raster imaging is performed by displacing the sample in X and Y directions every pixel resolution distance. In the case of this paper, the image pixels have been measured moving the sample every 254 µm, below the spatial resolution.

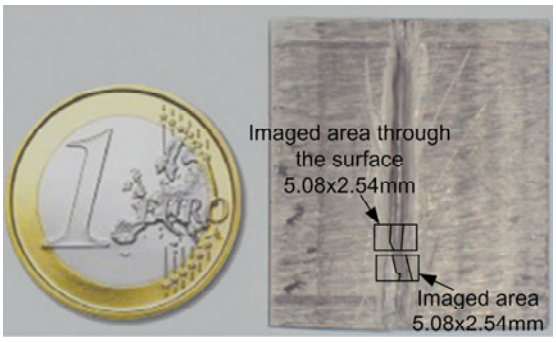

Fig.7: Photograph of the measured sample. Both imaged areas are illustrated on the photograph.

Fig. 7 shows the sample of ceramic dielectric material of relative permittivity ε_r= 13 (measured in X-band) used to perform the imaging. The dimensions of the sample are 29x33 mm and it has a thickness of 2.4 mm. A crack of approximately 2 mm of width has been cut on the surface with a depth of around 0.5 mm.

Two types of images have been obtained. First a surface image that gives information about the shape of the sample face in front of the lens has been retrieved. This image has been reconstructed by using the first reflection of the transmitted pulse. The second type of acquired image gives information about the shape of the opposite face of the sample. The second reflection of the transmitted pulse has been used to process the latter image.

Both measured areas are shown in Fig. 7, where the shape profile has been depicted to better understand the images of the following section.

B. Measurements analysis

In this section an analysis of the obtained measurements and images is carried out. Fig. 8 shows two reflected signals in temporal domain from two different pixel positions when looking at the front face. The blue line corresponds to a reflection of a surface pixel. The time reference has been taken on the maximum of this reflection. The green dotted line of the same graph shows the signal reflected on the crack. The latter is delayed by 3.5 ps, agreeing with a crack depth on the order of 0.5 mm. Furthermore, a significant reduction on the amplitude is observed between two reflections due to the scattering produced by the irregular shape of the crack.

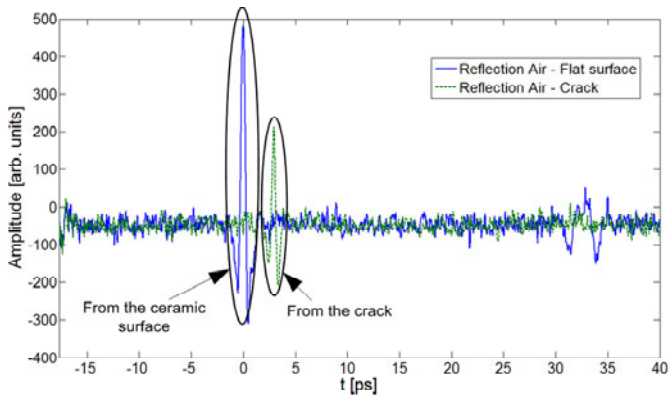

Fig.8: Reflected signals from a pixel on the surface of the sample and from a pixel on the crack (blue and green lines respectively).

Two images have been reconstructed using 20x10 pixel measurements. It has to be pointed out that the images have been interpolated in order to improve the perception of the shapes. Fig. 9 shows the surface shape of the sample around the crack, in the area depicted in Fig. 7. The processing of this image is based on taking the amplitude value at a fixed delay. In this case, to form the image the delay is 0. The contour shape of the crack is recovered, however the transitions are attenuated.

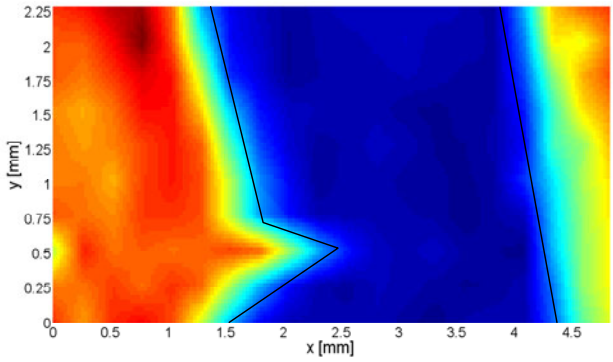

Fig.9: Image obtained when focusing to the surface of the sample

The Fig. 10 shows an image of the same area as Fig. 9 but in this case 3.5 ps of time delay has been used to retrieve the image. With this delay the picture gives information about the inner contour of the crack. This contour matches with the depicted crack shape of Fig. 7.

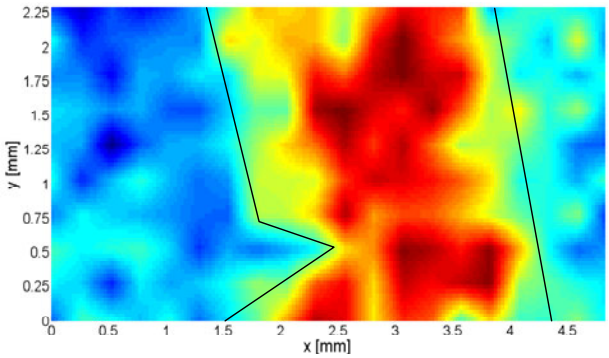

Fig.10: Image obtained when focusing to the crack on the opposite face

Fig. 10 uses the reflection between the sample material and the air at the opposite face in order to form the image. Fig. 11 shows the signal reflected in the transition from the surface to air in blue colour, whereas the signal reflected in the transition from the crack to the air is depicted in green. The time reference has been taken on the surface of the sample. A delay of 16 ps exists between both reflections. Using the relative permittivity of the material this delay is translated to 0.6 mm of crack depth.

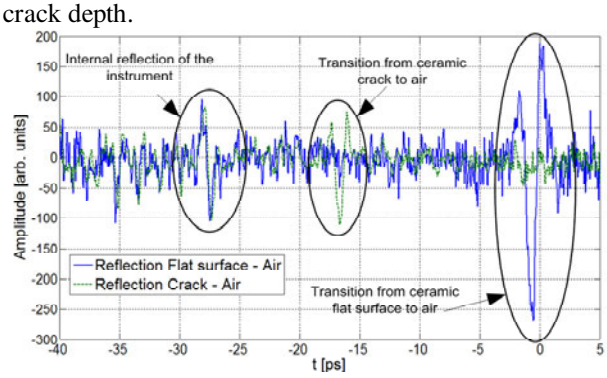

Fig.11: Reflected signals from a pixel on the opposite face of the sample and from a pixel on the crack (blue and green lines respectively).

Fig. 12 shows the reconstruction of the image using a time delay of 0. The shape of the surface in the opposite face is recovered. Now it has to be pointed out that the variations in the surface are better observed since the depth resolution is improved by a factor of $\sqrt{\varepsilon_r}$. Moreover the effect of the transitions becomes more noticeable.

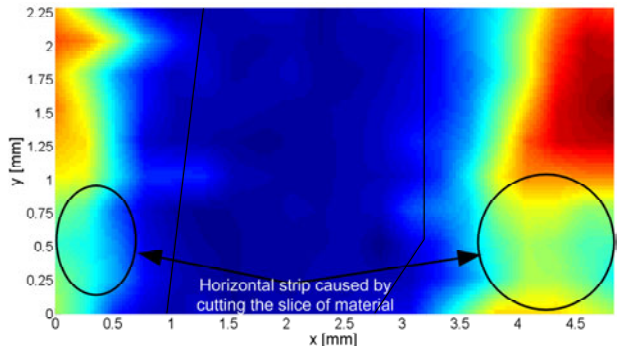

Fig.12: Image obtained when focusing to opposite face

Fig. 13 shows a reconstruction of the measured pixels when the delay applied is -16 ps. The crack shape is recovered. As in Fig. 12, the effect of the transitions is increased and only the stable surface of the crack is retrieved. This image proves the penetration capabilities of the terahertz radiation, being capable of penetrate 2.5 mm of high permittivity material with around 14 dB SNR averaging during 6 seconds. A full subsurface image of 20x10 pixels can be ideally recovered with this system in 20 minutes.

However, the measured pixels to obtain Fig. 9 and Fig. 10 have been averaged for 1 second, leading a measuring time of 200 s. This value is in accordance with the results presented in Fig. 5.

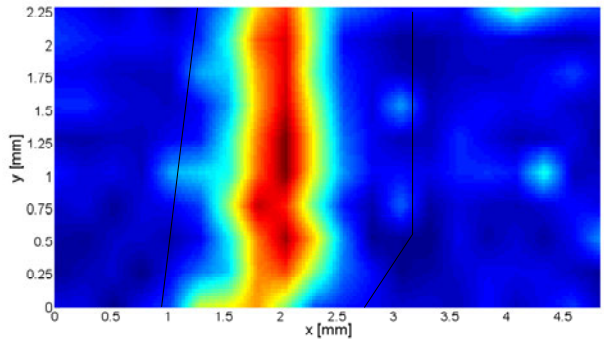

Fig.13: Image obtained when focusing to the crack on the opposite face

VI. Conclusions

A system based on a terahertz time-domain spectroscopy and capable of perform subsurface imaging in reflection using a retina has been proposed. Preliminary simulations have been carried out in order to show the imaging capabilities of the system. Moreover, a first calculation of the SNR of the system has been performed to foresee the acquisition time needed to form an image. The proof-of-concept of our system proposal

has been carried out using a commercial THz-TDS spectrometer. This system has been used to acquire images through a ceramic material, revealing the existence of a crack on the opposite face, and proving the penetration capabilities of the terahertz radiation.

ACKNOWLEDGMENT

We are grateful to Albert Redó, Gerard Salvatella and Regina Galceran from the *Universitat de Barcelona* for the received support on the utilization of the terahertz spectrometer.

This work was supported in part by Spanish CICYT under projects TEC2004-04866-C04-02 and TEC2007-66698-C04-01 and CONSOLIDER CSD2008-68.

REFERENCES

[1] E. Nova, J. Abril, M. Guardiola, S. Capdevila, A. Broquetas, J. Romeu, L. Jofre, *Terahertz Tomographic Imaging Technologies*, Proceedings of URSI-Spain 2009

[2] Bolomey, J. and Gardiol, F. E., *Engineering Applications of the Modulated Scatterer Technique*, Artech House, 2001

[3] Bedri A. Cetiner, Necmi Biyikli, *Penta-Band Planar Inverted F-Antenna (PIFA) Integrated by RF-NEMS Switches,* UGIM 2008

[4] Steven G. Johnson and John D. Joannopoulos, *MEEP freely available FDTD simulation software*, Massachusetts Institute of Technology

[5] Martin van Exter and Daniel R. Grischkowsky, *Characterization of an Optoelectronic Terahertz Beam System*, IEEE Trans. on Microwave Theory and Techniques, vol. 38, no. 11, 1990

[6] *Mini-Z terahertz time-domain spectrometer, Zomega corp., 2010*

Terahertz Spectroscopic Material Characterization and Imaging

E. Nova(1), J. Abril(1), J. Romeu(1), A. Broquetas(1), L. Jofre(1)
A. Redo-Sanchez(2), G. Salvatella(2), R. Galcerán(2)
enrique.nova@tsc.upc.edu , aredo@ub.edu
(1) Departament de Teoria del Senyal i Comunicacions. Universitat Politècnica de Catalunya
Jordi Girona 1-3, 08034 Barcelona
(2) Dpto. de Física Fundamental de la Universidad de Barcelona, C/ Martí Franquès 1, 08028 Barcelona

***Abstract*- A spectroscopic study of pharmaceutical substances has been performed in the THz frequency range using a commercial terahertz time-domain spectrometer (THz-TDS) configured in transmission mode. The measured samples have been already characterized in the terahertz frequency band, being the results available in the literature and used to validate our measurements. Furthermore, a subsurface imaging setup is presented using the THz-TDS spectrometer. A surface crack has been imaged through the surface of a ceramic material, thus verifying the penetration capabilities of the terahertz radiation on high dielectric materials.**

I. INTRODUCTION

Terahertz systems are nowadays accessible to chemical, alimentary and quality control laboratories. The price of such system has decreased due to the development and improvement of the femtosecond fiber laser, which currently is able to substitute the expensive Ti-sapphire femtosecond laser in many applications.

Moreover, automatic balancing and stability compensation techniques have been developed to control the correct alignment of the laser and terahertz beams through the entire spectrometer path. Therefore, the system does not need to be mounted on an optical table and is portable and compact.

The commercial spectrometer [1] used in our measurement setup includes the characteristics described above. It is compact, portable and can be placed in any position. Furthermore, the measurements can be carried out either in reflection or transmission geometry. The narrow pulses emitted by the spectrometer have a large spectral content approximately from 0.2 THz to 2 THz; hence images with depth resolution of few micrometers can be obtained using this system.

On the one hand, this system has been used to characterize the absorption resonances produced by the crystalline structures of pharmaceutical substances, such as dexchlorpheniramine maleate, riboflavin and diclofenac sodium.

On the other hand, surface and subsurface images from a dielectric material have been acquired, revealing the existence of a crack behind the surface of the material placed in front of the spectrometer.

II. SPECTROSCOPIC CHARACTERIZATION

A. Characterization setup and sample preparation

In order to perform absorption measurements, the spectrometer has been configured in transmission mode. In this configuration, the THz beam is focused on the sample, in a pellet form, with a combination of parabolic mirrors and polyethylene lenses. The samples have been prepared grinding the pharmaceutical substance into fine powder and mixing it with high density polyethylene (HDPE) to a total weight of 150 mg. Moreover, the mixture has been pressed with 20 tones of pressure to form a pellet of around 2 mm of thickness.

The spectrometer has been purged using nitrogen gas to minimize the water vapor effects, because water vapor presents a high radiation absorbance at THz frequencies. Fig. 1 shows two measurements of water vapor absorbance for two different values of humidity. This measurement has been carried out by modifying the environment humidity conditions while controlling its level using the humidity sensor, which is integrated on the system. Absorption peaks at 0.56 THz, 0.75 THz, 1.14 THz, 1.41 THz and 1.69 THz are obtained, agreeing with the results obtained in [2].

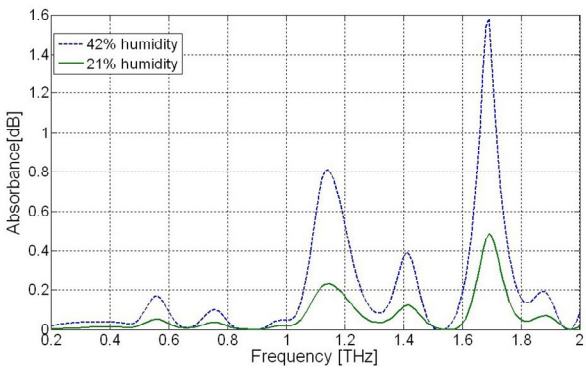

Fig. 1. Water absorption spectrum for 21% and 42 % of humidity.

The level of water vapor has been reduced to 2% after the purge. Afterwards, the noise level of the system has been measured blocking the terahertz beam, therefore, the detected signal is the noise from the receiver stage. Using the value of

noise, the dynamic range can be calculated. A reference measurement of the polyethylene pellets has been carried out in order to eliminate possible absorption lines introduced by this material. The noise and reference measurements are presented in Fig.2. From this picture, a dynamic range of 50 dB is obtained at 1 THz.

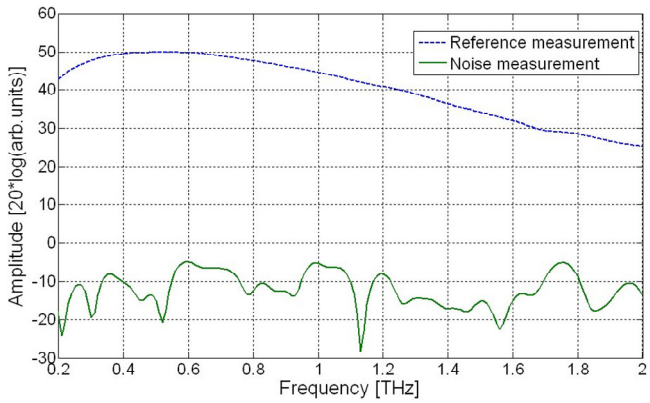

Fig. 2. Measurements of receiver noise and polyethylene reference.

B. *Data processing and results*

A baseline appears in the absorbance measurements. This baseline is created due to scattering effects on the material that are dependent on the frequency. In order to properly compare results from various concentrations of chemical substances, an algorithm is applied to remove the baseline.

Since the THz- TDS spectrometer gives information about the time evolution of the received pulse, the Fourier transform is calculated to obtain the spectrum. In order to retrieve the absorption characteristics of the sample, the obtained spectrum is corrected using the reference measurement. In this process, the contributions from the water vapor and from internal reflections are corrected.

Fig. 3 shows the absorbance curves for two different concentrations of dexchlorpheniramine maleate, a pharmaceutical substance obtained from the medicine Polaramine, which is an anti-histamine drug. The measurement presents three absorption peaks at 0.53 THz, 1.19THz and 1.38 THz.

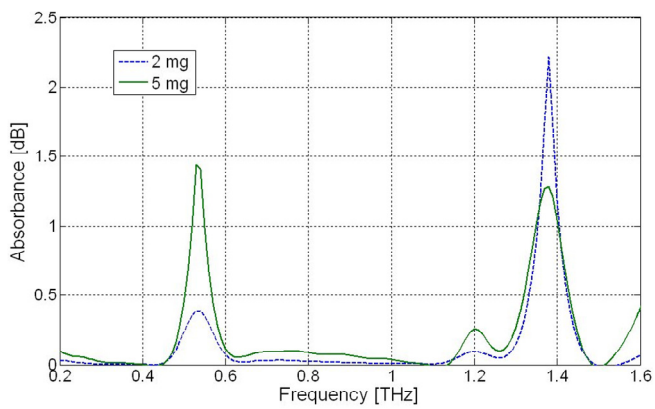

Fig. 3. Absorption spectrum of dexchlorpheniramine maleate.

However, it is probable that these absorption peaks are caused by $\alpha\text{-}lactose$, one of the pharmaceutical excipients used in the fabrication of the medicine. In [3][4] can be found studies of $\alpha\text{-}lactose$ with similar results of those obtained in the Fig. 3. In [5], a numerical study of the $\alpha\text{-}lactose$ molecule, results in a rotational mode at 0.525 THz, two translation modes at 0.993 THz and 1.110 THz , and a rotational mode at 1.32 THz.

Fig. 4 shows the absorption spectrum for two different quantities of diclofenac sodium. In this case, the sample does not contain excipients. Two absorption peaks are revealed at 0.96 THz and 1.35 THz. In this case, a clear dependence of the absorption with the quantity of the sample substance is observed.

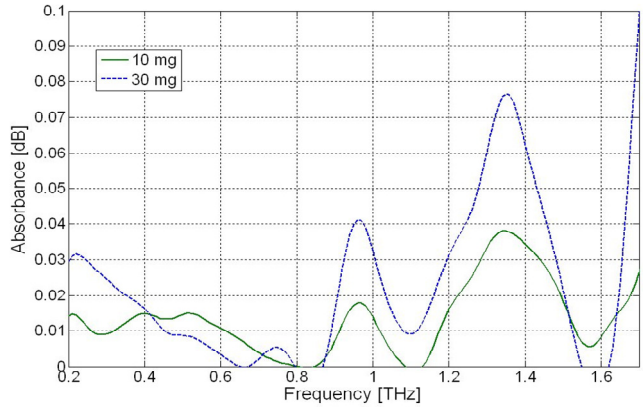

Fig. 4. Absorption spectrum of diclofenac sodium.

A measurement of a pure riboflavin, which is the B2 vitamin, sample has been carried out. Two different quantities of 10 mg and 30 mg have been measured. The obtained spectrums show a possible characteristic double peak close to 1.04 THz and 1.18 THz, and a third peak at 1.51 THz. Takahashi *et al.*, has measured riboflavin in the terahertz frequency band obtaining peaks at 1.03 THz, 1.18 THz and 1.52 THz [6].

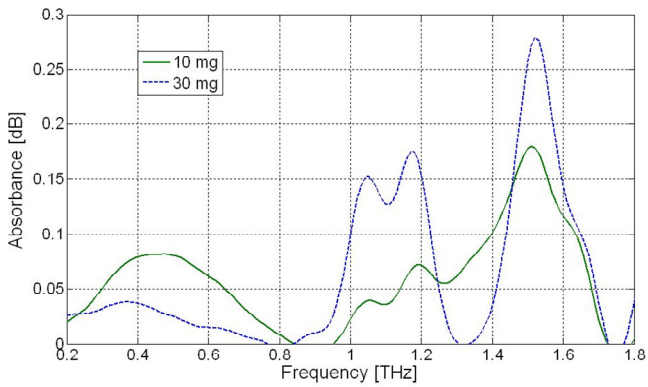

Fig. 5. Absorption spectrum of riboflavin.

III. TERAHERTZ SUBSURFACE IMAGING

A. Measurement setup

The spectrometer can be configured in reflection mode by placing an accessory module that transmits and receives the electromagnetic radiation using a unique lens. In this configuration, the system allows to acquire data in real time with a dynamic range of around 25 dB and a repetition rate greater than 7 Hz. This value of dynamic range can be further improved if the measurement is averaged. The depth resolution is approximately 75 µm, if 2 THz of pulse bandwidth are considered.

Fig. 6 shows the setup configuration used to acquire the images presented in the following section. An optical breadboard has been used to fix the spectrometer. The sample is held on 3D stage composed of three independent linear stages. The sample is displaced in the Z direction to place the surface of the focal point of the lens. At this point, the measured beam waist is 170 µm, leading a pixel resolution of 340 µm.

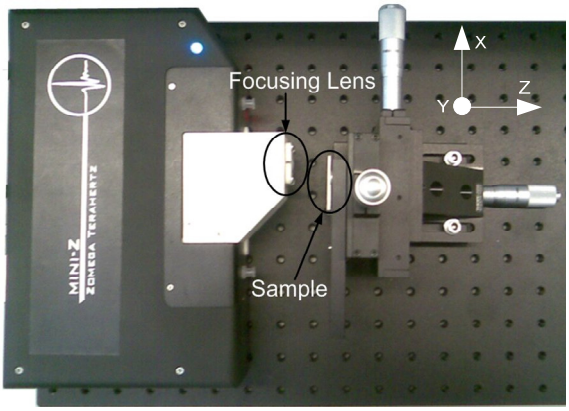

Fig. 6. Photograph of the setup geometry.

The raster imaging is performed by displacing the sample in X and Y directions each 254 µm, below the measured spatial resolution.

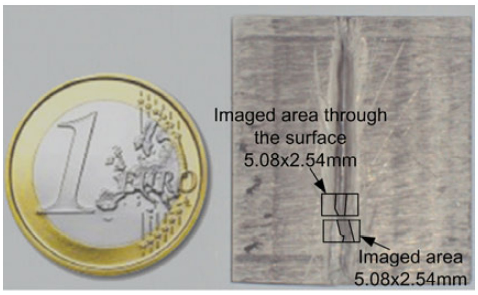

Fig. 7. Photograph of the ceramic block used as a sample. Both image areas are presented as rectangles in the photograph. The shape of the crack has been depicted on these areas.

Fig. 7 shows the sample of ceramic dielectric material of dielectric permittivity of $\varepsilon_r = 13$ (measured in X band). The dimensions of the sample are 29x33 mm with a thickness of 2.4 mm. A crack of approximately 2 mm of width has been cut on the surface with a depth of around 0.5 mm.

Two types of imaging have been performed. A surface image giving information about the sample topology in front of the lens has been obtained. In this case, the image has been reconstructed using the first reflection of the transmitted pulse. In the second type of imaging, the image has been acquired using the second reflection of the transmitted pulse. Therefore, this image gives information about the shape of the opposite face of the sample. Both measured areas are shown in Fig. 7, where the crack shape profiles help to understand the images presented in the following section.

B. Measurements analysis

The analysis of the obtained measurements and images is performed. Fig. 8 shows two reflected signals in temporal domain from two different pixel positions when looking at the front face of the sample. The blue line corresponds to a reflection produced when the focus of the lens is pointing to the flat surface whereas the red line corresponds to a reflection produced when the pixel retrieved is place inside the crack. The latter is delayed by 3.5 ps, agreeing with a crack depth on the order of 0.5 mm. Moreover, a significant reduction of the amplitude is observed between two reflections due to the scattering produced by the irregular shape of the crack.

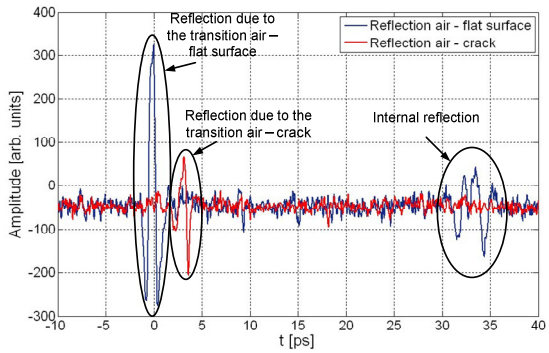

Fig. 8. Reflected signals from a pixel on the surface of the simple and from a pixel on the crack (blue and red lines respectively).

An image has been reconstructed using a 20x10 pixel measurement. Fig. 9 shows the surface shape of the sample around the crack. The processing of this image is based on taking for each pixel the amplitude value where the reflection produced by the transition air-flat surface occurs. The crack is observed with the shape depicted in Fig. 6.

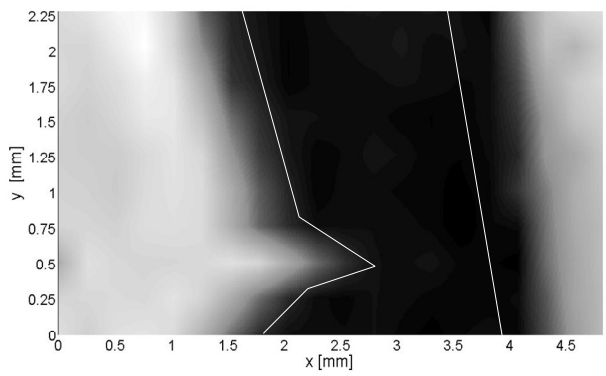

Fig. 9. Image obtained when using the first reflection on the sample surface.

Fig. 10 shows the signal reflected in the transition from the surface to the air in blue color, whereas the signal reflected in the transition from the crack to the air is depicted in green. A delay of 16 ps exists between both reflections. Using the relative permittivity of the material, this delay is translated to 0.6 mm of crack depth.

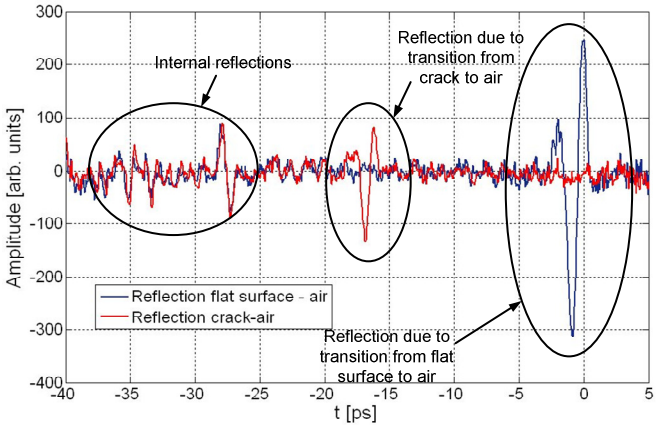

Fig. 10. Reflected signals from a pixel on the opposite face of the simple and from a pixel on the crack (blue and red lines respectively).

Fig. 11 shows a reconstruction of the measured pixels when the response is taken at the time instant of the reflection produced in the transition between the flat surface and the air. The crack shape is recovered. This image verifies the penetration capabilities of the terahertz radiation, being capable of penetrating 2.5 mm of high pemittivity material with around 14 dB of SNR averaging during 6 seconds. A full subsurface image of 20x10 pixels can be ideally recovered with this system in 20 minutes.

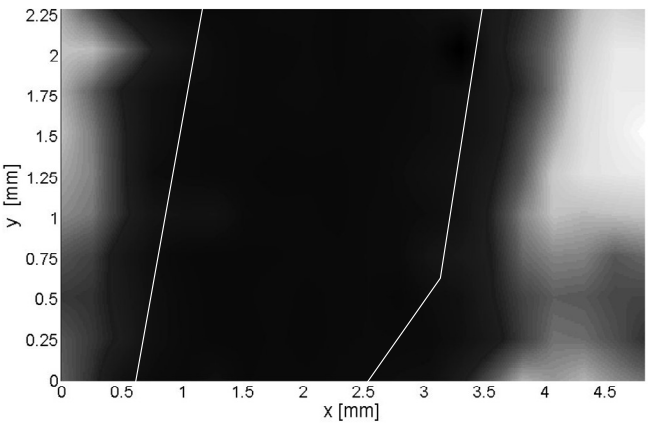

Fig. 11. Subsurface image obtained when using the second reflection in the opposite face of the sample.

IV. Conclusions

A commercial terahertz time-domain spectrometer has been used to perform a spectroscopic characterization of pharmaceutical substances. The spectral absorption lines of three pharmaceutical substances have been characterized from 0.2 THz to 2 THz. Moreover, a subsurface imaging setup has been built using the spectrometer in reflection configuration. To reconstruct an image of the surface of a ceramic material, the first reflection of the transmitted pulse has been used. Moreover, a subsurface image of the opposite face has been obtained using the reflection between the sample and the air, revealing the existence of the crack imaging through the surface with depth resolutions of 75 µm and an acquisition time of 20 minutes.

Acknowledgments

This work was supported in part by Spanish CICYT under projects TEC2004-04866-C04-02 and TEC2007-66698-C04-01 and CONSOLIDER CSD2008-68.

References

[1] *Mini-Z terahertz time-domain spectrometer,* Zomega corp., 2010

[2] Martin van Exter, Ch. Fattinger, and D. Grischkowsky, "Terahertz time-domain spectroscopy of water vapor" *Optic Letters,* Vol. 14, No. 20, October 15, 1989.

[3] E.R. Brown, J.E. Bjarnason, A.M. Fedor, and T.M. Korter. "On the strong and narrow absorption signature in lactose at 0.53 THz". *Applied PhysicsLetters,* 90:061908, 2007.

[4] M.Walther, M.R. Freeman, and F.A. Hegmann. "Metal-wire terahertz time-domai spectroscopy". *Applied Physics Letters*, 87:261107, 2005.

[5] S. Saito, T.M. Inerbaev, H. Mizuseki, N. Igarashi, N. Ryunosuke, and Y. Kawazoe. "First principles calculation of terahertz vibrational modes of a disaccharide monohydrate crystal of lactose" *Japanese Journal of Applied Physics*, 45(43):L1156–L1158, 2006.

[6] M. Takahashi, Y. Ishikawa, J. Nishizawa, and H. Ito. "Low-frequency vibrational modes of riboflavin and related compounds". *Chemical Physics Letters*, 401(4-6):475–482, 2005.

Combined Passive and Active Millimeter-Wave Imaging System for Concealed Objects Detection

J.Abril, E.Nova, A.Broquetas, F.Torres, J.Romeu L.Jofre
Remote Sensing Lab, Dpt. Signal Theory and Communications
Univeristat Politècnica de Catalunya

***Abstract*— In this paper, a comparison between both imaging techniques is performed with the aim of integrating both in a single imaging system. It is expected that the combination of the coherent and incoherent radiation in active and passive operation will offer improved detection and identification of concealed objects. An interferometric radiometer and an active mills-cross have been studied as near field imaging systems. The main parameters have been simulated to foresee their performance as image scanning systems. Moreover, a T-shape active imaging system has been built and measurements have been done in order to test and assess the performance of this imaging geometry.**

I. Introduction And Background

ACTIVE and passive imaging systems offer different advantages in terms of performance and scene visualization. The scene coherent illumination of active systems allows fast acquisition times, however the images are affected by speckle noise limiting its interpretation. On the other hand, passive systems receive the very weak signal radiated by the scene, needing large integration times to achieve proper radiometric sensitivities but are not affected by speckle noise.

Prior to the prototype development [1], several simulations have been performed for both system topologies to assess the requirements in terms of number of antennas, antenna spacing, required bandwidth and other performance parameters described in the following section.

To validate the concept a prototype has been developed; first we have focused on the active setup, due to the simpler implementation thanks to the use of the network analyzer either as a transmitter or receiver. The passive system which will be further combined with the active results is currently being developed.

The measurement results for the T-shape are shown in the last section of the paper. Comparing both the simulated and measured images, a similar behavior can be observed.

II. Geometry and Operation Principles

The scheme for the interferometric passive acquisition and image reconstruction is shown in Fig.1a. The system is based on a cross shape array which works in receiving mode and obtains an image of the apparent brightness temperature radiated by the scene under test. The array elements are followed by a downconverter to allow a digital correlation of the base-band noise corresponding to all the antenna pairs. Finally using an imaging algorithm that includes an appropriate compensation of the near-field phase distortion the image is obtained.

Fig.1b depicts the scheme of the active system, which uses the same sensing geometry. The vertical array elements are used sequentially in transmitting mode in order to illuminate the scene. For each transmitting antenna the scattered fields by the scene on the horizontal array elements are measured. The scattering matrix is processed by a computer in order to image the scene spatial domain with a focusing operator [2].

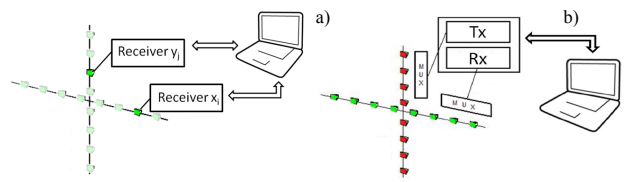

Fig.1: a) Passive configuration: Interferometric Radiometer b) Active configuration: Mills-Cross

III. Simulation Results

For the passive system the simulation scene, Fig.2, consists of a differential-temperature target of 1x1m. The array dimensions are 24.6 x 24.6 cm, working at 94GHz, antenna spacing of 1λ, and 77x77 antennas. The estimated resolution of the system is 1 cm at a distance of 1m. The shape of the objects can be recovered, showing the capability of the system to image the objects of interest.

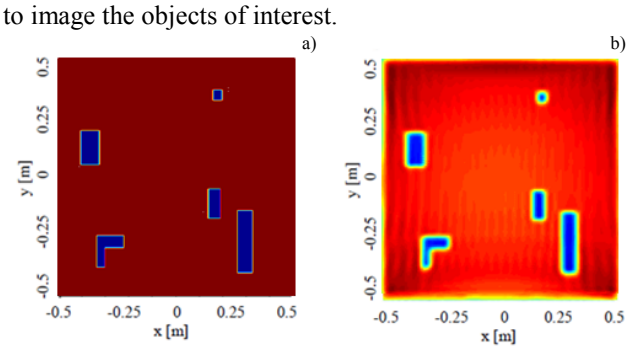

Fig.2: a) Target scene of 1x1m. b) Reconstructed image using 77 X-axis and 77 Y-axis antennas at a distance of 1 m.

For the active system the simulation scene, Fig.3, comprises the values of reflectivity for both the background and objects; following a Gaussian distribution and differing 6 dB. The array, as in the case of the passive setup, has 77x77 antennas. The original scene can be retrieved. However, due to the

coherent nature of the system performance, the speckle noise can be noticed.

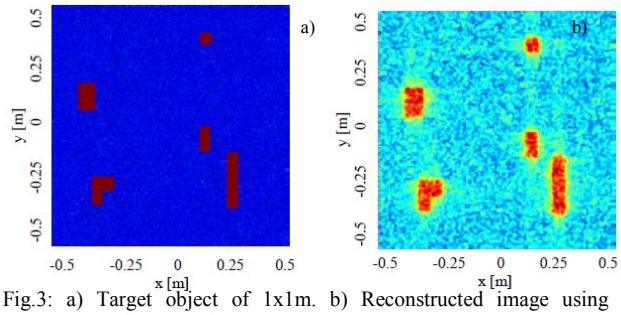

Fig.3: a) Target object of 1x1m. b) Reconstructed image using 77x77 antennas at a distance of 1 m.

IV. Measurement Setup

To assess the Mills-cross simulations results, a similar geometry of exploration has been implemented, a T-shape is used instead of a cross-shape. The reason for changing the array geometry is to avoid the crossing of the two axis in the laboratory implementation of the measurement set-up. Fig.4 shows the setup and the scene under test used to perform the measurements.

The scenario being imaged consists of a bottle of water performing as a human body, a file simulating a weapon, and a T-shirt covering the scene in order to conceal the target, as shown in Fig.4b. In this case the target is placed at a range distance of 35 cm.

The setup to perform the image reconstruction consists of a horizontal linear stage which moving in steps of a wavelength creates a synthetic linear array used in transmitting mode in order to illuminate the scene by means of the network analyzer (VNA). The transmitted power is amplified to 13dBm from 90 GHz to 98 GHz using a medium power amplifier. For each transmitting point the scattered fields by the scene on the synthetic vertical array are measured with the VNA. The total number of positions of each linear stage is 60, considering a spacing of 1λ, and a minimum wavelength of 3,06mm leads to a travel range of 18.3cm.

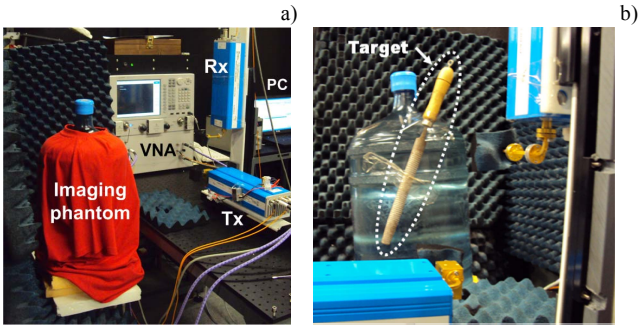

Fig.4. Imaging system based on a T-shape array. a) Geometry of exploration and imaging phantom. b) Scenario under test without the T-shirt, in order to visualize the target.

V. Measurement Results

Fig.5 a shows the recovered image obtained from measuring the phantom. A focusing algorithm is applied to retrieve the image using the full system bandwidth (90-98 GHz), including a Hamming windowing of the imaging aperture and a time gating. The aperture windowing is used in order to reduce the impact of the sidelobes on the image. However, it degrades the resolution of the system.

Moreover, a time gating is used to subtract the mutual coupling between both antennas. Only the received signal corresponding to a time interval including the reflection of the target is processed. With this method, the background noise is reduced and the appearance of undesired artifacts in the image is avoided.

In Fig.5a the retrieved image from the phantom is presented. A vertical straight line is seen in the image corresponding to the reflection of the frontal face of the water bottle. This strong reflection is produced due to the high permittivity of water in this frequency range.

An image of the file placed in front of the phantom and covered with a T-shirt is presented in Fig.6b. The T-shirt is penetrated and both the reflection of the water bottle and the reflection of the file are shown in the image.

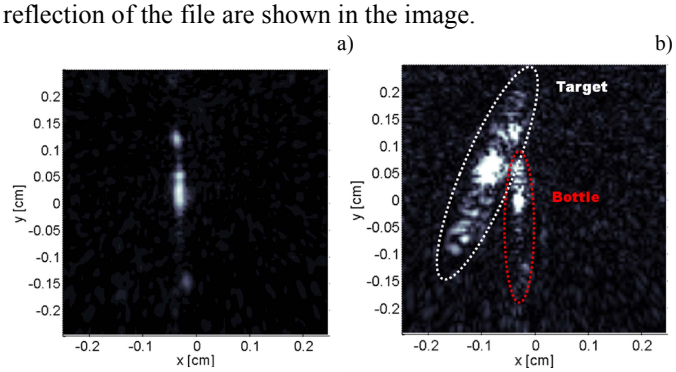

Fig.5. Retrieved images from two scenes: In a) only the phantom has been measured and processed whereas in b) a file is placed in front of the phantom and covered with a T-shirt.

VI. Conclusions

Two imaging systems approaches, active and passive, have been presented. Simulations for each setup have been performed in order to study the response of each geometry of exploration. The capability of the system in recovering the target has been validated.

Next work to be performed will focus on the interferometric radiometer measurements. Once fulfilled we will combine both results in such a way to improve the final retrieved images

References

[1] Markus Peichl, H. Suess, and M. Suess, "Microwave imaging of the brightness temperature distribution of extended areas in the near and far field using two-dimensional aperture synthesis with high spatial resolution", Radio Sciende, Volume 33, Number 3, May-June 1998.

[2] Antoni Broquetas, Josep Palau, Luis Jofre, Angel Cardama,"Wave Near-Field Imaging and Radar Cross-Section measurement" IEEE transactions on antennas and propagation, VOL. 46, NO. 5, MAY 1998.